Gas Evolution in Lithium-Ion Batteries: Solid versus Liquid Electrolyte

Florian Strauss,[†,*] Jun Hao Teo,[†] Alexander Schiele,[†] Timo Bartsch,[†] Toru Hatsukade,[†] Pascal Hartmann,[†,‡] Jürgen Janek,[†,§] and Torsten Brezesinski[†,*]

[†] Battery and Electrochemistry Laboratory, Institute of Nanotechnology, Karlsruhe Institute of Technology (KIT), Hermann-von-Helmholtz-Platz 1, 76344 Eggenstein-Leopoldshafen, Germany.

[‡] BASF SE, Carl-Bosch-Strasse 38, 67056 Ludwigshafen, Germany.

[§] Institute of Physical Chemistry & Center for Materials Science, Justus-Liebig-University Giessen, Heinrich-Buff-Ring 17, 35392 Giessen, Germany.

Abstract

Gas evolution in conventional lithium-ion batteries using Ni-rich layered oxide cathode materials presents a serious issue, responsible for performance decay and safety concerns, among others. Recent findings revealed gas evolution occurring also in bulk-type solid-state batteries. To further clarify the effect that the electrolyte has on gassing, we report in this work—to the best of our knowledge—the first study comparing gas evolution in lithium-ion batteries with NCM622 cathode material and different electrolyte types, specifically solid (β-Li_3PS_4 and Li_6PS_5Cl) versus liquid (LP57). Using isotopic labeling, acid titration, and *in situ* gas analysis, we show the presence of O_2 and CO_2 evolution in both systems, albeit with different cumulative amounts, and possible SO_2 evolution for the lithium thiophosphate-based cells. Our results demonstrate the importance of considering gas evolution in solid-state batteries, especially the formation and release of highly corrosive SO_2, due to side reactions with the electrolyte.

Keywords

Lithium-ion battery, all-solid-state battery, organic carbonate liquid electrolyte, lithium thiophosphate solid electrolyte, gas evolution, interfacial chemistry

TOC Graphic

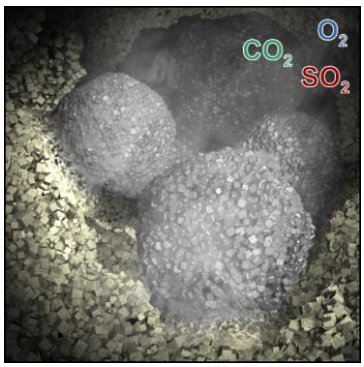

Introduction

Lithium-ion batteries (LIBs) are an indispensable energy storage technology nowadays, enabling the widespread use of portable electronics. In addition, and even more importantly, LIBs are key to the efforts toward transportation electrification.[1] State-of-the-art LIBs rely on layered lithium transition metal oxides as cathode, such as $Li_{1+x}(Ni_{1-y-z}Co_yMn_z)_{1-x}O_2$ (NCM), and graphite as anode in combination with an organic carbonate-based liquid electrolyte.

Increasing the fraction of redox-active Ni in NCM-type cathode materials has been shown a viable strategy for achieving specific capacities of ≥200 mAh/g_{NCM} in a reasonable voltage range.[2] However, the operation of such NCMs in liquid electrolyte-based LIBs (referred to as liq-LIBs in the following) causes the formation of gaseous side products, such as O_2, CO, and CO_2, among others, eventually leading to performance loss and safety issues.[3–5]

Various possible pathways of gas generation have been discussed in literature.[4–9] Firstly, the electrochemical oxidation of the organic electrolyte gives rise to CO and CO_2 evolution.[6] Secondly, the electrochemical decomposition of residual carbonate species, usually present on the surface of especially Ni-rich NCMs, leads to CO_2 and O_2 evolution, predominantly in the initial charge cycle.[9] Thirdly, the structural instability of Ni-rich NCMs at high states of charge (SOC) causes the release of lattice O_2, which chemically reacts with the liquid electrolyte, thereby producing CO and CO_2.[5,8]

As we have shown recently for bulk-type solid-state batteries (SSBs), similar gas evolution can also occur, along with unique SO_2 formation, when using lithium thiophosphate solid electrolytes.[10,11] Nevertheless, the effect of different thiophosphates on gas evolution is yet to be studied as well as how it compares to liq-LIBs. In this work, we present a comparative study to clarify such questions, focusing on the evolution of CO_2 and O_2 in liq-LIB and SSB cells and SO_2 in the latter using isotopic labeling combined with *in situ* gas analysis.

Experimental

Materials Preparation

For the synthesis of β-Li_3PS_4 solid electrolyte, stoichiometric amounts of Li_2S (Sigma Aldrich; 99+%) and P_2S_5 (Sigma Aldrich; 99%) in a 70 mL zirconia jar with 10-mm-diameter zirconia balls (~55:1 ball-to-powder ratio) were mixed under argon for 1 h at 250 rpm. Then, the mixing speed was increased to 650 rpm, and the milling was continued for 20 h. The resultant powder material had a conductivity of ~0.5 mS/cm.

For the synthesis of Li_6PS_5Cl solid electrolyte, Li_2S, P_2S_5, and LiCl (Alfa Aesar; 99+%) in a 250 mL zirconia jar with 10-mm-diameter zirconia balls were milled under argon for 1 h at 250 rpm and then for 20 h at 450 rpm. Subsequently, the harvested material was heated for 5 h at 300 °C in a vacuum. Note that (i) the ball-to-powder ratio was ~27:1, (ii) LiCl was predried overnight at 300 °C in a vacuum, and (iii) Li_2S was used in a less than stoichiometric amount (by 10 mol.%). The resultant powder material had a conductivity of ~2.0 mS/cm.

Regeneration of Cathode Material

$Li_{1+x}(Ni_{0.6}Co_{0.2}Mn_{0.2})_{1-x}O_2$ (NCM622, 60% Ni) cathode material (BASF SE; D_V^{50} = 5.19 µm, D_V^{90} = 9.04 µm) was heated in oxygen flow for 2 h at 740 °C to remove both native LiOH and Li_2CO_3 surface contaminants. The resultant powder material was stored under argon for further use.[3–5]

$Li_2{}^{13}CO_3$ Surface Layer Formation

For the formation of $Li_2{}^{13}CO_3$ on the cathode material's surface, regenerated (i.e., virtually Li_2CO_3-free) NCM622 was placed in a custom cell under a ~2.5 bar ^{13}C-labeled CO_2 atmosphere (Sigma Aldrich; 99 at.% ^{13}C).[12] The storage cell underwent purge cycles following its assembly to replace the initial argon atmosphere. In addition, 300 µL of H_2O was introduced into a cavity inside of the cell to accelerate the carbonate formation. Finally, it was placed in an oven for 2 h at 60 °C.

SSB Cell Assembly and Testing

All steps were performed under argon. The cathode composite was prepared in a 70 mL zirconia jar with 10-mm-diameter zirconia balls (~30:1 ball-to-powder ratio) by mixing either β-Li_3PS_4 or Li_6PS_5Cl solid electrolyte, NCM622 cathode material, and Super C65 carbon black additive (Timcal) in a 3:7:0.1 weight ratio for 30 min at 140 rpm. The SSB cells were assembled in a 10-mm-diameter PEEK ring, its use ensuring relatively high pressures to be applied onto the pellet without cracking or relaxation occurring. The ring was placed on a steel mold, allowing the powder to be sequentially pressed into pellets. First, 100 mg of solid electrolyte were compacted at ~125 MPa. Next, 13 mg of cathode composite (11−12 mg_{NCM}/cm^2, ~2.1 mAh/cm^2) were pressed by hand onto the solid electrolyte layer. Then, an 8-mm-diameter Al mesh was carefully placed onto the cathode composite, followed by compression at ~440 MPa. In addition, a 9-mm-diameter stainless steel mesh was placed onto the Al mesh/cathode layer to help promote connectivity. Subsequently, the PEEK ring was removed from the steel mold along with the solid electrolyte separator and cathode composite layers. Finally, a 100-µm-thick, 8-mm-diameter In anode (Alfa Aesar) was attached to the pellet, and the PEEK ring containing the assembled cell (with spacers on both sides) was introduced into the differential electrochemical mass spectrometry (DEMS) setup. The cathode spacer had 1-mm-diameter holes to ensure proper outflow of released gas during cycling. All SSB cycling [after leaving the cell at open circuit voltage (OCV) for 6 h] was done at a C/20 rate, with 1C = 180 mA/g_{NCM}, and at 45 °C in the potential range between 2.3 and 4.4 V versus In/InLi using a BioLogic VMP potentiostat.

Separating Solid Electrolyte and Cathode Material

To determine the carbonate content of the SSB cathode composite after mixing and after the initial cycle, the solid electrolyte had to be removed, as the strong H_2S evolution when using the acid titration setup (more details below) did not allow for accurate measurement of CO_2. Hence, ~30 mg of either cathode composite or cycled

SSB pellet were dispersed in 3 mL of N-methylformamide (Sigma Aldrich; NMF), able to dissolve the solid electrolyte while leaving Li_2CO_3 unaffected. The In anode was removed in the case of the cycled SSB pellet before dissolving in NMF. The NMF was carefully dried over activated molecular sieves (Merck); the H_2O content was determined to be ~2 ppm by Karl-Fischer titration. After pouring of the solution and repeated washing with NMF, the powder was dried for at least 24 h in a vacuum prior to acid titration measurement. The NCM622 cathode material with an artificially grown $Li_2{}^{13}CO_3$ surface layer served as reference sample and was treated in the same way as described above (to ensure the carbonate is not affected by the NMF).

Liq-LIB Cell Assembly and Testing

Electrodes were prepared with a composition of 94 wt.% NCM622 cathode material, 3 wt.% Solef5130 polyvinylidene fluoride binder (Solvay), and 1 wt.% Super C65 carbon black and 2 wt.% SFG6L graphite additives (Timcal). The areal loading was ~8.5 mg_{NCM}/cm^2. For DEMS, the liq-LIB cells were assembled inside an Ar-filled glovebox by stacking 600-µm-thick, 32-mm-diameter Li anode (Albemarle Germany GmbH), 36-mm-diameter Celgard 2500 polypropylene separator, and 30-mm-diameter NCM622 cathode. The latter electrode had 4 mm diameter holes in the middle for proper gas extraction and attachment of a Li reference electrode. 260 µL of LP57 (BASF SE; 1 M $LiPF_6$ in 3:7 by weight ethylene carbonate and ethyl methyl carbonate) was used as electrolyte. The cells were left at OCV for 6 h and then cycled at a C/10 rate (higher compared with the SSB cells due to experimental constraints), with 1C = 240 mA/g_{NCM}, and at 45 °C with a charge capacity limitation of 240 mAh/g_{NCM}. The cutoff potential on discharge was set to 3.0 V versus Li^+/Li.

Gas Characterization

The gas evolution was studied using DEMS by monitoring m/z = 1−100. Helium (purity 6.0, 2.5 mL/min) served as carrier gas for both the SSB and liq-LIB cells. The extracted gas was analyzed by a mass spectrometer (Pfeiffer Vacuum GmbH; OmniStar GSD 320). Additional information is provided in literature.[13,14]

Carbonate Determination

4−11 mg of NCM622 powder was introduced into a vial with a septum-sealed cap. Next, 1 M H_2SO_4 (Merck KGaA), degassed for 1 h through argon bubbling, was added. The reaction between Li_2CO_3 and H_2SO_4 releases CO_2, which was extracted from the vial using argon carrier gas (purity 6.0), controlled by a mass flow controller (Bronkhorst High-Tech BV; EL-FLOW Select) at 2.5 mL/min. The evolution of both $^{12}CO_2$ and $^{13}CO_2$ was monitored quantitatively by a mass spectrometer (Pfeiffer Vacuum GmbH; HiCube Pro with a PrismaPlus detector).

Results and Discussion

As mentioned previously, NCM622 (60% Ni) was used in this study as cathode material. To unequivocally prove the nature of evolved gasses, the native carbonate surface contaminants were first removed through 2 h treatment at 740 °C in flowing O_2, and then they were regrown in a controlled manner using isotopically pure $^{13}CO_2$. After drying the NCM622 overnight at 300 °C in a vacuum, acid titration coupled with mass spectrometry was carried out to determine the amount of carbonate species. The resultant $Li_2{}^{12}CO_3$ and $Li_2{}^{13}CO_3$ contents were 0.07 and 0.76 wt.%, respectively, corresponding to ~92% ^{13}C.

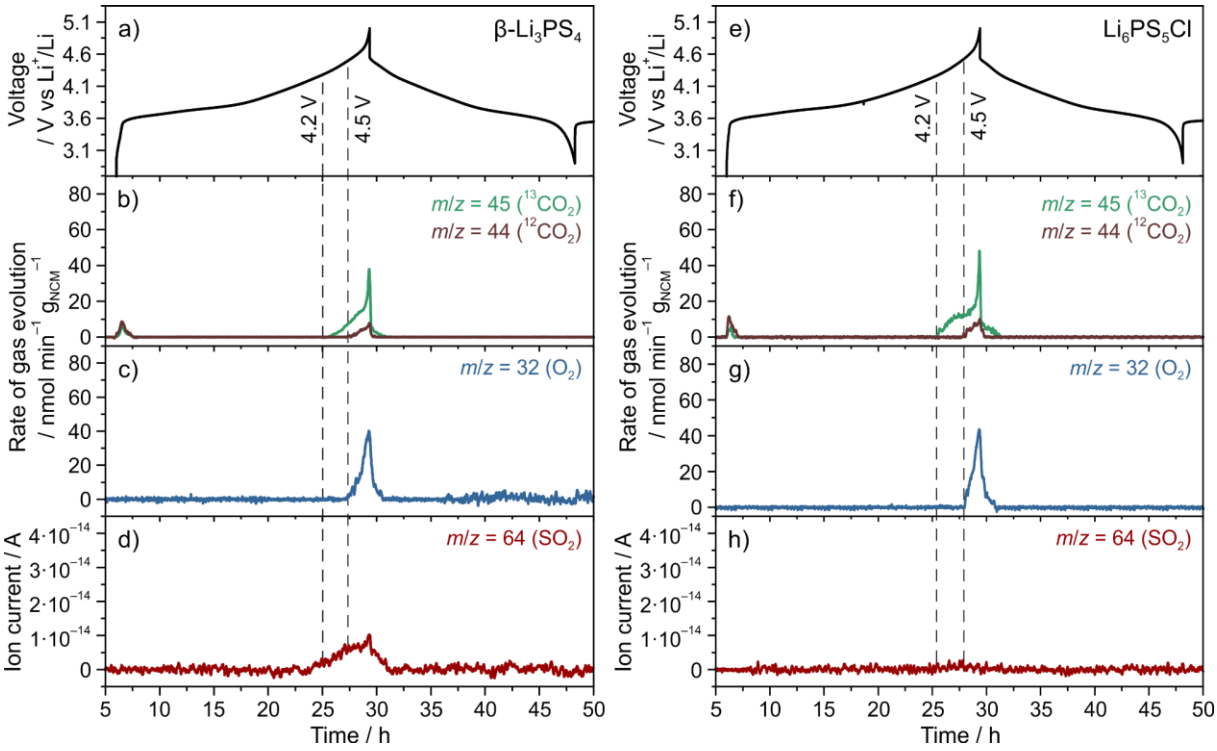

Figure 1. Electrochemical trace of SSB cells using (a) β-Li_3PS_4 and (e) Li_6PS_5Cl solid electrolyte and the corresponding time-resolved (b, f) $^{12}CO_2$, $^{13}CO_2$ and (c, g) O_2 evolution rates and (d, h) ion current for SO_2. The cells were cycled in the potential range of 2.3−4.4 V with respect to In/InLi (~2.9−5.0 V vs Li^+/Li).

Next, SSB and liq-LIB cells were assembled, and the gas evolution in the initial cycle was monitored using DEMS (mass signals from *m*/*z* = 1−100). The setup employed is described in some more detail in literature.[10,13,14] In a first step, SSB cells with β-Li_3PS_4, NCM622, and In as solid electrolyte, cathode, and anode, respectively, were examined. They were cycled at a rate of C/20 and 45 °C between 2.3 and 4.4 V versus In/InLi, corresponding to ~2.9−5.0 V with respect to Li^+/Li. As is evident from **Figure 1a**, the electrochemical trace is characteristic of Ni-rich NCM, with first cycle specific charge and discharge capacities of 210 and 170 mAh/g_{NCM}. Regarding gas evolution, two signals with *m*/*z* = 44 and 45, referring to $^{12}CO_2$ and $^{13}CO_2$, respectively, were clearly visible near the end of the charge cycle (**Figure 1b**). The $^{13}CO_2$ evolution can be attributed to the electrochemical decomposition of $Li_2{}^{13}CO_3$ on the NCM622 surface, the onset being ~4.2 V versus Li^+/Li, in agreement with literature.[5,9,15] However, the

onset of $^{12}CO_2$ evolution was ~300 mV higher in potential compared with that of $^{13}CO_2$. An explanation might be that the native carbonate contaminants can only be partially removed from the NCM622 secondary particles during the regeneration process, especially those that are present in the interior of the material. At high potentials or SOC, the particles typically undergo some fracture, which may release $^{12}CO_2$. However, oxidation of Super C65 carbon black additive, present in the cathode composite, cannot be excluded.

Minor CO_2 formation was also observed in the beginning of the initial charge cycle, probably because of side reactions occurring at the interface of In anode and solid electrolyte separator. This hypothesis relies on the fact that the CO_2 onset potential is strongly correlated with that of H_2 (m/z = 2), the latter of which appears as a sharp peak (**Figure S1**). H_2 evolution may be related to trace H_2O reduction in the cell.[6,10] However, we believe that it is also associated with the solid electrolyte and the released H_2 is capable of somewhat reacting with the carbonate species, thereby forming CO_2.[16] In addition, the onset potentials of $^{12}CO_2$ and $^{13}CO_2$ evolution (in the beginning of charging) were found to be identical within the experimental error, arguing for a chemical rather than an electrochemical reaction. In this context, it should be noted that no H_2S (m/z = 34) evolution was detected, suggesting either complete removal of trace H_2O during the initial reduction or insensitivity of the solid electrolyte to very low levels of H_2O (**Figure S1**). In any case, the lack of H_2S evolution indicates that H_2O-related effects are negligible in these experiments.

Moreover, a sharp peak for m/z = 32, referring to O_2, was visible at the end of charge, the onset potential being ~4.5 V versus Li^+/Li (**Figure 1c**). The O_2 evolution can originate from two different sources as proposed in literature, either its release from the NCM lattice or the electrochemical decomposition of Li_2CO_3 (note that for the Li_6PS_5Cl-based SSB cells, the apparent molar ratio of CO_2:O_2 is of the order of 2:1 expected for the latter reaction).[9,15,17] Both sources seem reasonable here. However, the release of O_2 from the NCM lattice requires the SOC to be ≥80% (100% refers to full delithiation).[17] The initial specific charge capacity was 210 mAh/g_{NCM}, which is equivalent to ~76% SOC. Hence, one would not expect to observe any O_2 evolution. Nevertheless, as demonstrated recently for SSBs, inhomogeneities in SOC may be present during cycling. In other words, occurrence of cathode material fractions possessing different SOC is possible,[18–20] and thus some of the NCM622 particles may exceed 80% SOC, eventually leading to O_2 loss.

Lastly, a trace for m/z = 64 (SO_2) was observed (**Figure 1d**), a unique feature that has been reported so far only for SSB cells using β-Li_3PS_4 solid electrolyte.[10,11] The most obvious route leading to SO_2 formation and release is the reaction between O_2 and the solid electrolyte, accompanied by formal sulfur oxidation, along with the formation of solid oxygenated sulfur and phosphorus species as confirmed by X-ray photoelectron spectroscopy (XPS) and time-of-flight secondary ion mass spectrometry (ToF-SIMS), among others.[21–24] As mentioned above, two sources of O_2 are generally possible, namely O_2 released from the NCM lattice or through the electrochemical decomposition of Li_2CO_3. Having in mind that the evolved O_2 during cycling appears to be partially or completely highly reactive $^1O_2$,[15,25,26] a gas/solid reaction may even occur

at 45 °C, despite a recent report that surface oxidation of lithium thiophosphates (by $^3O_2$) requires much higher temperatures.[27] The DEMS data, especially the result that the SO_2 evolution begins/stops simultaneously with the $^{13}CO_2$ evolution (during charge and discharge at ~4.2 V vs Li^+/Li), support such reaction mechanism.

Given the apparent effect of lithium thiophosphate solid electrolytes on the gassing behavior, we subsequently substituted β-Li_3PS_4 for argyrodite Li_6PS_5Cl in an otherwise identical SSB. Cycling of such cells under the same conditions resulted in gas evolution characteristics of $^{12}CO_2$, $^{13}CO_2$, and O_2 (**Figure 1e-g**), similar to those for β-Li_3PS_4. However, a clear distinction was observed for SO_2 (**Figure 1h**). In contrast to β-Li_3PS_4, there was no SO_2 evolution, thereby suggesting higher chemical stability of Li_6PS_5Cl toward reaction with $^1O_2$ and/or formation of only solid decomposition products. Note that its lower electrochemical stability does not necessarily affect the gas evolution.[28,29] In all cases of Li_6PS_5Cl samples, SO_2 peaks in the raw data were indistinguishable from the background. Moreover, if any peaks were observed, the ion current was usually much lower compared with the β-Li_3PS_4 samples and they did not correspond to the timeframe where other characteristic gasses (CO_2 and O_2) evolved. For both types of SSB cells, the evolution of gases detected during the initial cycle was also seen for the second and third cycles, although with decreased intensity (**Figures S2** and **S3**).

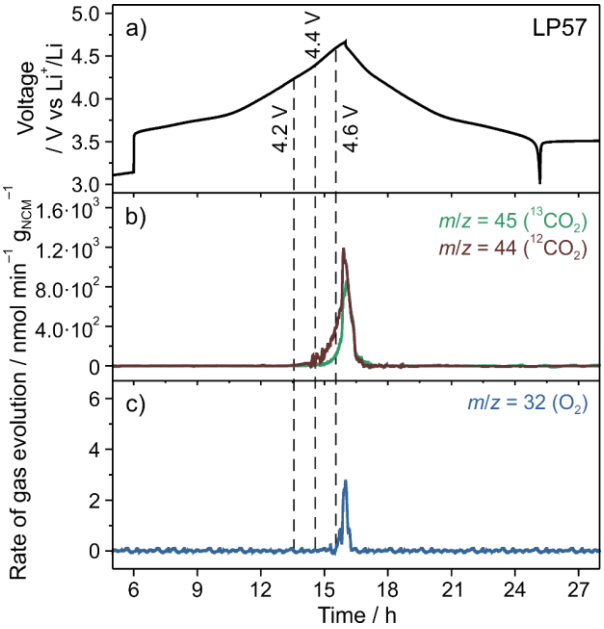

Figure 2. (a) Electrochemical trace of a liq-LIB cell cycled using a charge capacity limitation of 240 mAh/g_{NCM} and the corresponding time-resolved (b) $^{12}CO_2$, $^{13}CO_2$ and (c) O_2 evolution rates.

Thus far, we have shown that gas evolution related to CO_2, O_2, and partially SO_2 occurs in battery cells depending on the electrolyte used. To compare gassing in such systems in a more detailed manner, conventional liq-LIBs using tape-cast electrodes with the same NCM622 cathode material and LP57 electrolyte were assembled. The cells were cycled at a rate of C/10 and 45 °C with a charge capacity limitation of 240 mAh/g_{NCM} (~87% SOC). The voltage profile is displayed in **Figure 2a**. As shown in **Figure 2b**,

both $^{12}CO_2$ and $^{13}CO_2$ evolution at the end of charge/beginning of discharge can be spotted, with onset potentials of ~4.2 and ~4.4 V versus Li^+/Li, respectively. This result indicates that decomposition of LP57 electrolyte occurs prior to Li_2CO_3 decomposition, in agreement with literature.[5,17] At first sight, in contrast to the SSB cells, the quantity of evolved $^{12}CO_2$ seems greater than that of $^{13}CO_2$, which can be attributed to the additional contribution from the (electro)chemical decomposition of the carbonate-based liquid electrolyte, accounting for $^{12}CO_2$ formation (note that, because of the isotopic labeling, Li_2CO_3 decomposition is mainly responsible for $^{13}CO_2$ evolution).[5,9,30] Moreover, in line with previous literature reports, O_2 evolution arises at an onset potential of ~4.6 V versus Li^+/Li (**Figure 2c**), referring to ~83% SOC.[17] We also observed H_2 and CO evolution (**Figure S4**), typically originating from the reductive decomposition of the liquid electrolyte and/or trace water.[6] However, with their maximum amplitude occurring near the end of charge, it is more likely that these are stemming from oxidative electrolyte decomposition processes, with CO being a direct product[12,17] and H_2 an indirect product, arising from the reduction of protic species that are formed at the positive electrode and diffuse to the negative electrode.[6] The apparent time-shift between the peaks of CO and H_2 (with H_2 evolving slightly later than CO) supports this hypothesis.

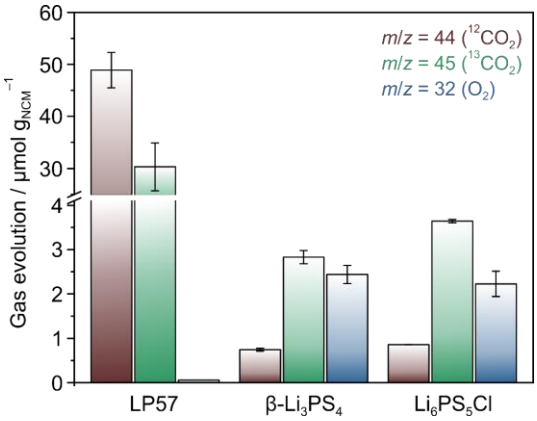

Figure 3. Total quantity of $^{12}CO_2$, $^{13}CO_2$, and O_2 evolved during the initial charge/discharge cycle at 45 °C of SSB and liq-LIB cells. Error bars indicate the standard deviation of two independent measurements.

Because the SSB and liq-LIB cells show common CO_2 and O_2 evolution, the total quantity of evolved gases in the initial cycle can be compared (**Figure 3**). Note that the liq-LIBs were charged using a specific capacity limitation of 240 mAh/g_{NCM} to achieve a similar SOC to the SSBs. Although the latter cells showed slightly lower specific capacities, ranging from 210 to 230 mAh/g_{NCM}, inhomogeneities in SOC of the NCM622 particles, especially for pelletized SSB cells, are inevitable,[18–20] warranting such comparison.

First of all, in the case of the LP57 electrolyte, the $^{12}CO_2$ amount was significantly larger (~49 µmol/g_{NCM}), compared to ~1 µmol/g_{NCM} for the SSB cells. As mentioned above, this is because of decomposition of the carbonate-based liquid electrolyte, mainly contributing to $^{12}CO_2$ formation. As the carbonate surface species were labeled with ^{13}C, $^{13}CO_2$ evolution can be attributed unambiguously to the electrochemical

decomposition of Li_2CO_3. For the liq-LIB cells, about an order of magnitude more $^{13}CO_2$ evolved compared with the SSB cells (~30 vs 3−4 μmol/g_{NCM}). We suspect that this difference is due to (i) better ionic and electronic percolation in the liq-LIB electrode and/or (ii) trapping of CO_2 by the solid electrolyte (pore blocking or physisorption/chemisorption) and/or (iii) formation of solid side products in the case of the SSB cells. The fraction of $^{12}CO_2$ to the total quantity of evolved CO_2 [$^{12}C/(^{12}C+^{13}C)$] was ~0.08 in the pristine ^{13}C-labeled NCM622 (from acid titration measurements). However, for the first cycle gas evolution, it was much larger than expected at ~0.18 (from DEMS measurements).The reason is unclear at present but may be related to the unique surface structure and/or partial oxidation of Super C65 carbon black in the SSB cathode composites.

Moreover, the amount of released O_2 was similar for the different SSB cells (~2 μmol/g_{NCM}). For the liq-LIB cells, it was more than an order of magnitude lower. Nevertheless, in the case of the LP57 electrolyte, the virtually total consumption of released O_2 through side reactions with the carbonate liquid electrolyte, leading to $^{12}CO_2$ and CO formation, among others, must be taken into account.[17,30] Note that such phenomenon is also responsible for the occasional absence of the O_2 signal (below the detection limit). Similar reactions seem to occur for the SSB cells. This means that part of the released $^1O_2$ undergoes follow-up reactions, either leading to formation of SO_2 or solid products as mentioned above, however, not as pronounced as for the liq-LIB cells because gas/liquid reactions tend to be kinetically favored over gas/solid reactions.

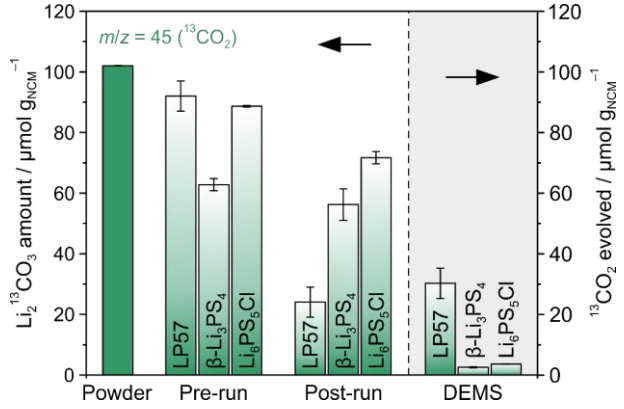

Figure 4. Amount of $Li_2{}^{13}CO_3$ on the NCM622 cathode material before and after cycling from acid titration measurements compared to the cumulative amount of $^{13}CO_2$ from DEMS. Error bars indicate the standard deviation of two independent measurements.

Li_2CO_3 contaminants on Ni-rich and Li/Mn-rich cathode materials have been recognized lately to account for CO_2 evolution, especially during the initial cycle of liq-LIBs, and also to be responsible for $^1O_2$ formation.[9,12,15] Both to further clarify the role of such surface residuals in the CO_2 release and to identify unique characteristics for the SSB cells, we quantitatively determined the amount of Li_2CO_3 present on the NCM622 cathode material by acid titration measurements prior to and after cycling (**Figure 4** and **Table S1**) and compared this with the DEMS results. We only focus on $^{13}CO_2$, as ^{13}C is the major species within the surface layer after tailored formation of

$Li_2{}^{13}CO_3$, and thus can be considered representative for the carbonate contaminants in this case. The amount of artificially grown $Li_2{}^{13}CO_3$ on the NCM622 particles was determined to be ~102 µmol/g_{NCM}. After electrode preparation (referred to as pre-run), this initial value was strongly decreased to ~63 µmol/g_{NCM} for β-Li_3PS_4 and slightly decreased to ~89 and ~92 µmol/g_{NCM} for Li_6PS_5Cl and the tape-cast electrodes used in the liq-LIB cells, respectively. This implies that some of the carbonate species on the NCM622 surface react with the β-Li_3PS_4 solid electrolyte during preparation of the cathode composite, forming gaseous and/or solid side products. However, their nature remains elusive at present. After the initial cycle (referred to as post-run), a further reduction in $Li_2{}^{13}CO_3$ amount, because of electrochemical decomposition, was observed in all cases. Note that chemical decomposition due to reaction with HF, for example, is also feasible for the liq-LIB cells. In particular, it diminished to ~56, ~72, and ~24 µmol/g_{NCM} for β-Li_3PS_4, Li_6PS_5Cl, and LP57 electrolyte, respectively. This foremost suggests higher connectivity between the NCM622 particles and the electrolyte in the liq-LIB cells (i.e., better electrochemical addressability of the active material and therefore $Li_2{}^{13}CO_3$), which does not come as a surprise though, as inhomogeneities pertaining to inactive (electrically isolated) cathode material in pelletized SSB cells have been reported.[18–20] Moreover, this observation is in line with recent reports that most of the carbonate surface species are decomposed during the initial cycle for liq-LIBs.[9,12]

Adding up the total quantity of evolved $^{13}CO_2$ from DEMS and the amount of $Li_2{}^{13}CO_3$ deduced from acid titration measurements after the initial cycle (post-run) should yield a similar amount of $Li_2{}^{13}CO_3$ to that obtained for the as-prepared cathodes (pre-run). However, there are apparent discrepancies, ranging from <15% for β-Li_3PS_4 and Li_6PS_5Cl to ~40% for the LP57 electrolyte. Such discrepancies are probably because of differences in reactivity of the electrolytes tested and/or partial solubility of CO_2 in the case of the liquid electrolyte. In addition, the altered local environment of ^{13}C in the tape-cast electrodes, resulting from the presence of graphite additive and polyvinylidene difluoride binder, may also play a role.

Conclusions

In summary, we have shown common CO_2 and O_2 evolution upon cycling of LIB cells using a Ni-rich layered oxide cathode material (NCM622) and either a liquid (LP57) or solid electrolyte (β-Li_3PS_4 or Li_6PS_5Cl). Both species originate from the electrochemical decomposition of Li_2CO_3 surface contaminants and/or O_2 release from the NCM lattice at high SOC. Oxidative decomposition of the liquid electrolyte also contributes to CO_2 evolution in the liq-LIB cells, amounting to a significant share of the total quantity of evolved gases. From a numbers perspective, the cumulative amount of gases released during the initial cycle is more than an order of magnitude larger for the liq-LIB than SSB cells. Moreover, we show that SO_2 evolution may occur in lithium thiophosphate-based SSBs, its origin being related to the chemical reaction between O_2, probably $^1O_2$, and the solid electrolyte.

In a wider context, our work broadens the picture of the implications of gas evolution in LIBs. From an application perspective, gassing of SSBs appears to be less critical

than for liq-LIBs, since far less gaseous species are generated during cycling. However, the effect that solid electrolytes and especially surface-modified active materials can have on the gassing behavior calls for future studies to explore the complex interplay between interface/interphase formation and impedance buildup, among others.

Associated Content

Supporting Information

The Supporting Information is available free of charge on the ACS Publications website. Additional results from acid titration measurements and from DEMS for the liq-LIB and SSB cells.

Author Information

Corresponding Authors

*Phone: +49 721 60828907; Email: florian.strauss@kit.edu

*Phone: +49 721 60828827; Email: torsten.brezesinski@kit.edu

ORCID

Florian Strauss: 0000-0001-5817-6349

Jun Hao Teo: 0000-0002-0343-669X

Toru Hatsukade: 0000-0001-9016-0929

Jürgen Janek: 0000-0002-9221-4756

Torsten Brezesinski: 0000-0002-4336-263X

Present Address

A.S.: Carl Zeiss AG, Carl-Zeiss-Strasse 22, 73447 Oberkochen, Germany.

T.Ba.: VARTA AG, Alfred-Krupp-Strasse 9, 73479 Ellwangen, Germany.

T.H.: Argonne National Laboratory, 9700 South Cass Avenue, Lemont, IL 60439, USA.

Notes

The authors declare no competing financial interest. F.S. and J.H.T. contributed equally to this work.

Acknowledgments

This study is part of the projects being funded within the BASF International Network for Batteries and Electrochemistry. The authors also acknowledge the Federal Ministry of Education & Research (BMBF) for funding within the project ARTEMYS (03XP0114J).

References

(1) Larcher, D.; Tarascon, J.-M. Towards Greener and More Sustainable Batteries for Electrical Energy Storage. *Nat. Chem.* **2015**, *7*, 19−29.

(2) Myung, S.-T.; Maglia, F.; Park, K.-J.; Yoon, C. S.; Lamp, P.; Kim, S.-J.; Sun, Y.-K. Nickel-Rich Layered Cathode Materials for Automotive Lithium-Ion Batteries: Achievements and Perspectives. *ACS Energy Lett.* **2017**, *2*, 196−223.

(3) Kong, W.; Li, H.; Huang, X.; Chen, L. Gas Evolution Behaviors for Several Cathode Materials in Lithium-Ion Batteries. *J. Power Sources* **2005**, *142*, 285−291.

(4) Imhof, R. Novak, P. Oxidative Electrolyte Solvent Degradation in Lithium-Ion Batteries: An In Situ Differential Electrochemical Mass Spectrometry Investigation. *J. Electrochem. Soc.* **1999**, *146*, 1702−1706.

(5) Jung, R.; Metzger, M.; Maglia, F.; Stinner, C.; Gasteiger, H. Chemical vs. Electrochemical Electrolyte Oxidation on NMC111, NMC622, NMC811, LNMO, and Conductive Carbon. *J. Phys. Chem. Lett.* **2017**, *8*, 4820−4825.

(6) Metzger, M.; Strehle, B.; Solchenbach, S.; Gasteiger, H. A. Origin of H_2 Evolution in LIBs : H_2O Reduction vs. Electrolyte Oxidation. *J. Electrochem. Soc.* **2016**, *163*, A798−A809.

(7) Berkes, B. B.; Schiele, A.; Sommer, H.; Brezesinski, T.; Janek, J. On the Gassing Behavior of Lithium-Ion Batteries with NCM523 Cathodes. *J. Solid State Electrochem.* **2016**, *20*, 2961−2967.

(8) Jung, R.; Metzger, M.; Maglia, F.; Stinner, C.; Gasteiger, H. A. Oxygen Release and Its Effect on the Cycling Stability of $LiNi_xMn_yCo_zO_2$ (NMC) Cathode Materials for Li-Ion Batteries. *J. Electrochem. Soc.* **2017**, *164*, A1361−A1377.

(9) Renfrew, S. E.; McCloskey, B. D. Residual Lithium Carbonate Predominantly Accounts for First Cycle CO_2 and CO Outgassing of Li-Stoichiometric and Li-Rich Layered Transition Metal Oxides. *J. Am. Chem. Soc.* **2017**, *139*, 17853−17860.

(10) Bartsch, T.; Strauss, F.; Hatsukade, T.; Schiele, A.; Kim, A.-Y.; Hartmann, P.; Janek, J.; Brezesinski, T. Gas Evolution in All-Solid-State Battery Cells. *ACS Energy Lett.* **2018**, *3,* 2539−2543.

(11) Kim, A.-Y.; Strauss, F.; Bartsch, T.; Teo, J. H.; Hatsukade, T.; Mazilkin, A.; Janek, J.; Hartmann, P.; Brezesinski, T. Stabilizing Effect of a Hybrid Surface Coating on a Ni-Rich NCM Cathode Material in All-Solid-State Batteries. *Chem. Mater.* **2019**, *31,* 9664−9672.

(12) Hatsukade, T.; Schiele, A.; Hartmann, P.; Brezesinski, T.; Janek, J. Origin of Carbon Dioxide Evolved during Cycling of Nickel-Rich Layered NCM Cathodes. *ACS Appl. Mater. Interfaces* **2018**, *10*, 38892−38899.

(13) Berkes, B. B.; Jozwiuk, A.; Sommer, H.; Brezesinski, T.; Janek, J. Simultaneous Acquisition of Differential Electrochemical Mass Spectrometry and Infrared

Spectroscopy Data for In Situ Characterization of Gas Evolution Reactions in Lithium-Ion Batteries. *Electrochem. Commun.* **2015**, *60*, 64−69.

(14) Berkes, B. B.; Jozwiuk, A.; Vračar, M.; Sommer, H.; Brezesinski, T.; Janek, J. Online Continuous Flow Differential Electrochemical Mass Spectrometry with a Realistic Battery Setup for High-Precision, Long-Term Cycling Tests. *Anal. Chem.* **2015**, *87*, 5878−5883.

(15) Mahne, N.; Renfrew, S. E.; McCloskey, B. D.; Freunberger, S. A. Electrochemical Oxidation of Lithium Carbonate Generates Singlet Oxygen. *Angew. Chem. Int. Ed.* **2018**, *57*, 5529−5533.

(16) Lux, S.; Baldauf-Sommerbauer, G.; Siebenhofer, M. Hydrogenation of Inorganic Metal Carbonates: A Review on Its Potential for Carbon Dioxide Utilization and Emission Reduction. *ChemSusChem* **2018**, *11*, 3357−3375.

(17) Jung, R.; Metzger, M.; Maglia, F.; Stinner, C.; Gasteiger, H. A. Oxygen Release and Its Effect on the Cycling Stability of $LiNi_xMn_yCo_zO_2$ (NMC) Cathode Materials for Li-Ion Batteries. *J. Electrochem. Soc.* **2017**, *164*, A1361−A1377.

(18) Bartsch, T.; Kim, A.-Y.; Strauss, F.; de Biasi, L.; Teo, J. H.; Janek, J.; Hartmann, P.; Brezesinski, T. Indirect State-of-Charge Determination of All-Solid-State Battery Cells by X-Ray Diffraction. *Chem. Commun.* **2019**, *55,* 11223−11226.

(19) Strauss, F.; Bartsch, T.; de Biasi, L.; Kim, A.-Y.; Janek, J.; Hartmann, P.; Brezesinski, T. Impact of Cathode Material Particle Size on the Capacity of Bulk-Type All-Solid-State Batteries. *ACS Energy Lett.* **2018**, *3*, 992−996.

(20) Chen, K.; Shinjo, S.; Sakuda, A.; Yamamoto, K.; Uchiyama, T.; Kuratani, K.; Takeuchi, T.; Orikasa, Y.; Hayashi, A.; Tatsumisago, M.; Kimura, Y.; Nakamura, T.; Amezawa, K.; Uchimoto, Y. Morphological Effect on Reaction Distribution Influenced by Binder Materials in Composite Electrodes for Sheet-Type All-Solid-State Lithium-Ion Batteries with the Sulfide-Based Solid Electrolyte. *J. Phys. Chem. C* **2019**, *123*, 3292−3298.

(21) Koerver, R.; Aygün, I.; Leichtweiß, T.; Dietrich, C.; Zhang, W.; Binder, J. O.; Hartmann, P.; Zeier, W. G.; Janek, J. Capacity Fade in Solid-State Batteries: Interphase Formation and Chemomechanical Processes in Nickel-Rich Layered Oxide Cathodes and Lithium Thiophosphate Solid Electrolytes. *Chem. Mater.* **2017**, *29*, 5574−5582.

(22) Strauss, F.; Stepien, D.; Maibach, J.; Pfaffmann, L.; Indris, S.; Hartmann, P.; Brezesinski, T. Influence of Electronically Conductive Additives on the Cycling Performance of Argyrodite-Based All-Solid-State Batteries. *RSC Adv.* **2020**, *10*, 1114−1119.

(23) Auvergniot, J.; Cassel, A.; Ledeuil, J.-B.; Viallet, V.; Seznec, V.; Dedryvère, R. Interface Stability of Argyrodite Li_6PS_5Cl toward $LiCoO_2$, $LiNi_{1/3}Co_{1/3}Mn_{1/3}O_2$, and $LiMn_2O_4$ in Bulk All-Solid-State Batteries. *Chem. Mater.* **2017**, *29*, 3883−3890.

(24) Walther, F.; Koerver, R.; Fuchs, T.; Ohno, S.; Sann, J.; Rohnke, M.; Zeier, W. G.; Janek, J. Visualization of the Interfacial Decomposition of Composite

Cathodes in Argyrodite-Based All-Solid-State Batteries Using Time-of-Flight Secondary-Ion Mass Spectrometry. *Chem. Mater.* **2019**, *31*, 3745−3755.

(25) Freiberg, A. T.; Roos, M. K.; Wandt, J.; de Vivie-Riedle, R.; Gasteiger, H. A. Singlet Oxygen Reactivity with Carbonate Solvents Used for Li-Ion Battery Electrolytes. *J. Phys. Chem. A* **2018**, *122*, 8828−8839.

(26) Wandt, J.; Freiberg, A. T. S.; Ogrodnik, A.; Gasteiger, H. A. Singlet Oxygen Evolution from Layered Transition Metal Oxide Cathode Materials and Its Implications for Lithium-Ion Batteries. *Mater. Today* **2018**, *21*, 825−833.

(27) Sasaki, I.; Komori, T.; Honda, K.; Hibino, J. Enhancement of Rate Capability for All-Solid-State Batteries Using Surface Oxidized Sulfide Solid Electrolyte. *Electrochem. Soc.* AiMES **2018** Meeting, Cancun, Mexico.

(28) Richards, W. D.; Miara, L. J.; Wang, Y.; Kim, J. C.; Ceder, G. Interface Stability in Solid-State Batteries. *Chem. Mater.* **2016**, *28*, 266−273.

(29) Zhu, Y.; He, X.; Mo, Y. Origin of Outstanding Stability in the Lithium Solid Electrolyte Materials: Insights from Thermodynamic Analyses Based on First-Principles Calculations. *ACS Appl. Mater. Interfaces* **2015**, *7*, 23685−23693.

(30) Jung, R.; Strobl, P.; Maglia, F.; Stinner, C.; Gasteiger, H. A. Temperature Dependence of Oxygen Release from $LiNi_{0.6}Mn_{0.2}Co_{0.2}O_2$ (NMC622) Cathode Materials for Li-Ion Batteries. *J. Electrochem. Soc.* **2018**, *165*, A2869−A2879.